Geotechnical Testing Journal

doi:10.1520/GTJ20210100 / Vol. 45 / No. 1 / 2022 / available online at www.astm.org

Rodrigo Cesar Pierozan,[1] Abdurrahman Almikati,[2] Gregorio Luis Silva Araujo,[3] and Jorge Gabriel Zornberg[4]

Optical and Physical Properties of Laponite for Use as Clay Surrogate in Geotechnical Models

Manuscript received April 18, 2021; accepted for publication July 2, 2021; published online September 23, 2021. Issue published January 1, 2022.

[1] Department of Civil & Environmental Engineering, Pontifical Catholic University of Rio de Janeiro, 225 Marques de Sao Vicente St., Room 301, Rio de Janeiro, BR 22451-900, Brazil (Corresponding author), e-mail: rodrigopierozan@hotmail.com, https://orcid.org/0000-0002-2585-0840

[2] Department of Civil and Environmental Engineering, American University of Beirut, PO Box 11-0236, Riad El-Solh, Beirut 1107-2020, Lebanon, https://orcid.org/0000-0001-9686-6244

[3] Department of Civil and Environmental Engineering, The University of Brasilia, Darcy Ribeiro Campus, L3 North Rd., Building SG-12, Brasilia 70910-900, Brazil, https://orcid.org/0000-0003-4524-8846

[4] Department of Civil, Architectural and Environmental Engineering, The University of Texas at Austin, 301 E. Dean Keeton St., Room ECJ 9.227G, Austin, TX 78712, USA, https://orcid.org/0000-0002-6307-1047

Reference

R. C. Pierozan, A. Almikati, G. L. S. Araujo, and J. G. Zornberg, "Optical and Physical Properties of Laponite for Use as Clay Surrogate in Geotechnical Models," *Geotechnical Testing Journal* 45, no. 1 (2022): 79–100. https://doi.org/10.1520/GTJ20210100

ABSTRACT

Laponite has emerged as a particularly promising material for use as a soft clay surrogate in geotechnical modeling, as it provides a relevant range of transparency, plasticity, and overall geotechnical behavior. This paper presents an investigation of the significant factors affecting the transparency of laponite for its use in physical geotechnical models. Image analysis techniques and complementary optical tests were conducted to gain an understanding of the factors causing changes in optical clarity. Aging time, laponite content, and rheological additive dosage were found to be the most significant factors affecting the transparency of laponite. Specifically, the ratio between the rheological additive dosage and laponite content (additive mass ratio) was found to serve as a relevant index to define the material's optical behavior, and its use facilitated the determination of the optimum laponite and additive contents. The presence of inclusions within the internal laponite structure, such as trapped air pockets and unhydrated laponite crystals, identified as the key factor compromising optical clarity, could be ultimately associated with the selection of insufficient dosages of rheological additive. Overall, laponite was identified as a viable surrogate of natural clays suitable for models requiring comparatively large in-depth visualization.

Keywords

transparent clay, laponite, rheological additive, transparency, optical clarity, geotechnical model

Introduction

The use of transparent synthetic soils in laboratory testing procedures has emerged as a nonintrusive technique for the visualization of internal displacements (e.g., Iskander

2010). Granular transparent aggregates have included the use of amorphous silica gel (e.g., Iskander, Sadek, and Liu 2002; Toiya, Hettinga, and Losert 2007) and fused quartz (e.g., Ezzein and Bathurst 2011, 2014; Guzman, Iskander, and Bless 2015; Ferreira and Zornberg 2015; Kong et al. 2016; Peng and Zornberg 2017, 2019; Xiang et al. 2018; Chen et al. 2019; Yuan et al. 2020). On the other hand, transparent clay surrogates have involved the use of amorphous silica powder (e.g., Gill and Lehane 2001; Iskander, Liu, and Sadek 2002; Sadek, Iskander, and Liu 2002, 2003; Liu, Iskander, and Sadek 2003; McKelvey et al. 2004; Iskander and Liu 2010; Liu and Iskander 2010; Ni, Hird, and Guymer 2010; Black 2015; De Guzman and Alfaro 2016, 2018) and synthetic magnesium lithium phyllosilicate (e.g., Beemer and Aubeny 2012; Wallace, Rutherford, and Zheng 2015; Ads, Iskander, and Bless 2020).

Synthetic magnesium lithium phyllosilicate (Ads, Iskander, and Bless 2020), also known as laponite, has been reported to offer several advantages when used as transparent surrogate clay in geotechnical physical models, including adequate ranges of plasticity, rheology, and transparency (Wallace and Rutherford 2015). The use of laponite requires that adequate visibility extends to depths relevant to the problems being analyzed, thus ensuring testing accuracy, precision, and resolution (White, Take, and Bolton 2003). However, several inherent characteristics of laponite may affect its optical clarity (OC), including the laponite content, additive dosage, and inclusions that may develop within laponite microstructure (e.g., Beemer et al. 2016). Overall, the state-of-the-art in laponite modeling would benefit from a comprehensive quantification of the factors affecting the optical and related physical characteristics of hydrated laponite.

Previous efforts to evaluate transparency in geotechnical models have included the use of reference grid lines (e.g., Liu and Iskander 2010), eye chart assessment methods (e.g., Ads, Iskander, and Bless 2020), digital photography methods (e.g., Black and Take 2015; Beemer et al. 2016; Nelsen 2018), and adapted optical frameworks (Yi et al. 2018). Despite the significant insight provided by prior investigations, limited information is available on the quantification of transparency for comparatively large models.

The focus of the research presented in this paper is on laponite as a synthetic clay material as well as on the rheological additives used to reach a range of geotechnical properties representative of soft clays. An important objective is to investigate and quantify relevant factors affecting the transparency of laponite used as clay surrogate in physical modeling. The paper includes an initial discussion on available information on laponite, followed by a discussion on the impact of sample preparation and laponite recycling procedures. The optical and physical properties of laponite are subsequently discussed, including fabric and possible causes of decreased transparency. A method developed to assessing transparency is described, followed by an evaluation of the effect on transparency of the laponite content, rheological additive dosage, aging time, and depth of viewing plane.

Background on Laponite and Relevant Additives

Laponite is a synthetic smectite with structure and composition similar to those of the natural clay mineral hectorite (e.g., Thompson and Butterworth 1992; Ruzicka and Zaccarelli 2011). More specifically, laponite is a synthetic hydrophilic layered silicate that is insoluble in water but hydrates and swells when water is readily available. Laponite types are typically grouped into gel- and sol-forming additives, with both types having been utilized in applications such as construction, personal care, agriculture, polymers, surface coating, and paper (Kumar, Muralidhar, and Joshi 2008). The molecular formula of laponite (Balnois, Durand-Vidal, and Livitz 2003), which reflects the relative proportion between the chemical components (sodium, silicon, magnesium, lithium, fluorine, oxygen, and hydrogen), is as follows:

$$Na^{+}_{0.7}[(Si_8Mg_{(6-x)}Li_xF_y)O_{20}(OH)_{(4-y)}]^{-0.7} \quad (1)$$

where:

x = relative proportion of lithium, dimensionless, and

y = relative proportion of fluorine, dimensionless.

The advantages of using laponite as a transparent clay surrogate include efficient reproducibility, purity, and availability, rendering it suitable as a filler and thickening agent for aqueous preparations in a wide range of

industrial applications (Thompson and Butterworth 1992). Among the available laponite types, the gel-forming grades have been often adopted as a soft soil surrogate in geotechnical modeling. Specifically, this product is commercially known as Laponite-RD, being simply referred to as laponite in subsequent sections of this paper. The molecular formula of laponite powder (Laponite-RD), considering its average chemical composition (van Olphen 1977), corresponds to relative proportions x and y in equation (1) of 0.55 and 0, respectively. That is:

$$Na^{+}_{0.7}[(Si_8Mg_{5.45}Li_{0.3})O_{20}(OH)_4]^{-0.7} \quad (2)$$

Figure 1 illustrates different scales of the laponite structure. Laponite corresponds to a layered hydrous magnesium silicate within the family of (2:1) phyllosilicates (Ruzicka and Zaccarelli 2011). The unit cell is composed of 6 octahedral magnesium ions sandwiched between double layers of 4 tetrahedral silicon ions, as represented in **figure 1*A***. In powder form (**fig. 1*B***), laponite crystals share interlayer sodium ions (Na^+), resulting in highly oriented packed platelets (Ramsay, Swanton, and Bunce 1990). Laponite nanoparticles are hydrophilic and highly influenced by the pH level of the surrounding medium.

Once dispersed in water (for pH < 11), hydration reactions begin, and laponite particles show significant swelling (Ruzicka and Zaccarelli 2011). Release of sodium ions results in a highly negative charge on the laponite basal faces, while a weakly positive charge develops on the rims of the disks due to protonation of the hydroxyl groups (OH^-) with hydrogen atoms of water (Tawari, Koch, and Cohen 2001; Ruzicka, Zulian, and Ruocco 2006; Ruzicka and Zaccarelli 2011). This creates a colloidal dispersion of randomly oriented (Ramsay, Swanton, and

FIG. 1 General view and unit cells of laponite: (*A*) diagrammatic sketch of atomic structure; (*B*) laponite powder and arrangement into stacks; and (*C*) laponite in liquid and hydrated forms showing details of particle arrangements.

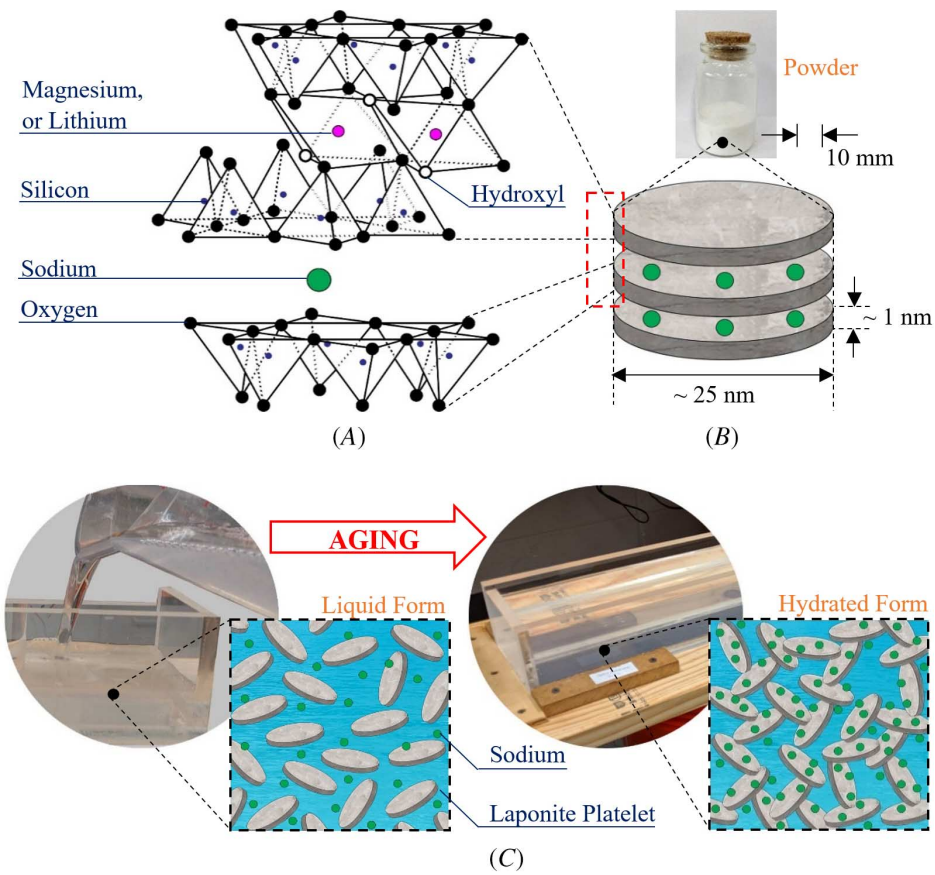

Bunce 1990) disk-shaped laponite particles with a thickness of ~1 nm and diameter of ~25 nm (Kumar et al. 2008; Ruzicka and Zaccarelli 2011), which are smaller than natural clay particles (Terzaghi, Peck, and Mesri 1996; Mitchell and Soga 2005). Such dispersion is illustrated in **figure 1C** (liquid form).

The workability of laponite samples for geotechnical physical modeling can be improved by reducing interactions among individual laponite particles to prevent gelation during sample preparation. This includes the use of the inorganic compound tetrasodium pyrophosphate ($Na_4P_2O_7$), as firstly suggested by Beemer et al. (2016). A laponite content of up to 13.5 % (Ads, Iskander, and Bless 2020) and 15 % (Beemer et al. 2016) has been achieved when using sodium pyrophosphate decahydrate ($Na_4P_2O_7.10H_2O$, designated as SPP) as a rheological additive. When dissolved in water, the tetravalent negatively charged pyrophosphate ions neutralize the positively charged rims of individual laponite particles, thus decreasing the electrostatic attractions between positively charged rims and negatively charged particle surfaces. Although this leads to decreased flocculation and reduced shear strength, it also results in improved workability by delaying gelation.

The aqueous laponite dispersion undergoes structural evolution and aging, which is characterized by a time-dependent increase in viscosity and modulus (Bonn et al. 1999). Electrostatic and van der Waals interactions develop between laponite platelets (Tawari, Koch, and Cohen 2001). Hydration results in a strongly interactive viscoelastic gel containing partially oriented platelets (Ramsay, Swanton, and Bunce 1990) due to the electrostatic attraction between the negatively charged faces and positively charged sides of the disks (Bonn et al. 1999), also designated as a "house of cards" structure (van Olphen 1977), which is represented in **figure 1C** (hydrated form). The effective volume associated with each laponite particle is much larger than the platelet itself (Mossa, Michele, and Sciortino 2007) because of the electrostatic screening on its surfaces.

Transparent soils have often been achieved by saturating a transparent aggregate with a pore fluid of matching refractive index, thus creating a homogeneous medium to light (e.g., Iskander and Liu 2010; Yuan et al. 2020). Commercially available laponite powder has a refractive index of 1.5000 (Wallace and Rutherford 2015), whereas the refractive index of pure distilled water (de-aired, at 20°C) is 1.3333 (Hecht 2017). Despite the mismatch of refractive indexes, each individual laponite platelet hydrates and swells in contact with water, so the refractive index of the resulting dispersion (which is time-dependent) ranges from 1.3345 to 1.3365 at 20°C (Kumar et al. 2008), thus creating a transparent material after hydration.

Hydrated laponite has a cellular microstructure with interconnected voids and is composed of elongated cells that are several orders of magnitude larger than natural clay particles (e.g., El Howayek et al. 2014; Ads, Iskander, and Bless 2020). This structure is characterized by a thixotropic behavior that shows an elastic response at rest and a viscoelastic or viscous response when subjected to shaking or shear loads caused by bonding breakings (Barnes 1997). When such loads end, the structure reverts to its original arrangement, also known as rebuild strength capability. A chemical dissociation occurs when hydrated laponite meets atmospheric carbon dioxide (CO_2), which results in leaching of magnesium ions (Mg^{2+}) into the solution (Ruzicka, Zulian, and Ruocco 2006), also influencing the OC and geotechnical properties of aged samples.

Materials Used in the Experimental Program

SPP was the rheological additive used throughout this study. This material was produced by Acros Organics, with a reported bulk density of 1,820 kg/m^3, a refractive index of 1.4250, and solubility in water of 62 g/L at 20°C. Laponite-RD, produced by BYK Additives and Instruments, was used as clay simulant. This material met the following specifications: bulk density of 1,000 kg/m^3; surface area of 370 m^2/g, according to the Brunauer–Emmett–Teller (BET) model; and refractive index of 1.5 at 20°C.

The chemical composition (dry basis), as reported by the supplier (BYK Additives and Instruments), consisted of 59.5 % of silicon (SiO_2), 27.5 % of magnesium (MgO), 2.8 % of sodium (Na_2O), and 0.8 % lithium (Li_2O). The coefficients describing the relative proportion of the chemical components of laponite (x and y in equation (1)) could be defined based on the reported composition. Accordingly, fluorine content is null (coefficient y), while the relative proportion of lithium corresponds to 0.55 (coefficient x). Therefore, the chemical

composition of the laponite used in the present study agrees with grade RD (equation (2)), as suggested by van Olphen (1977).

SAMPLE PREPARATION

The sample preparation methods adopted in this study are discussed next, including a brief discussion of the rationale for their selection and the approach adopted for sample remixing.

Protocols for Sample Preparation

Previous investigations have indicated that temperature influences considerably the transparency of soil surrogates such as fused quartz (Ezzein and Bathurst 2011) and amorphous silica (Black and Take 2015). Likewise, the temperature has also been reported to influence the rate of gelation of laponite (e.g., Ramsay 1986; Kumar et al. 2008). A constant temperature of 20°C was maintained in this study during sample preparation to facilitate the repeatability of test results.

The type of water adopted in this research was distilled water (de-aired, type II), which meets the specifications outlined in ASTM D1193-06(2018), *Standard Specification for Reagent Water*. Its reported refractive index is 1.3333 at 20°C (Hecht 2017). It should be noted that different types of water have been used in previous studies involving laponite, including tap water (e.g., Beemer et al. 2016; Ads, Iskander, and Bless 2020), de-aired distilled water (e.g., Chini et al. 2015; Wallace, Rutherford, and Zheng 2015; Wallace and Rutherford 2015), and deionized water (e.g., Ruzicka and Zacarelli 2011; Ads, Iskander, and Bless 2020), with pure sources of water being preferred for their comparatively low percentage of impurities.

Vigorous mixing at a fixed time interval has been recommended to facilitate proper laponite hydration and facilitate repeatability in experimental results (Ruzicka, Zulian, and Ruocco 2006; Ruzicka and Zaccarelli 2011). Nonetheless, unhydrated laponite aggregate crystals have been identified within the internal structure of laponite in gel form (e.g., Bonn et al. 1999; Nicolai and Cocard 2000), which has been attributed to incomplete mixing. The boundaries formed between unhydrated crystals and hydrated laponite may result in light scattering, which ultimately compromises OC. Different types of mixing devices have been used for laponite preparation, including an axial flow approach, recommended by laponite's manufacturer (BYK Additives and Instruments) to minimize sedimentation of solids (McConville and Kessler 2019).

Figure 2 displays this mixing system adopted in this study, with **figure 2*A*** showing the axial flow equipment and accessories used to mix the laponite aqueous solution, **figure 2*B*** depicting the 45° pitched blade turbine (with a diameter of 50 mm), and **figure 2*C*** showing the shape factors considered for the batch tank, i.e., bottom clearance (B_c), impeller diameter (D_i) and thickness (w), tank diameter (D_t), and liquid height (Z). The geometric ratios adopted in this study followed recommendations for adequate mixing of solids ($D_i/D_t = 1/3$, $w/D_i = 1/5$, $Z/D_t = 1$, $B_c/D_i = 1$) as reported by McConville and Kessler (2019).

The oven-dried mass of SPP and laponite (m_{SPP} and m_{lap}, respectively) were determined by discounting the masses of water, as estimated by the water content values (68 % and 8.2 % for SPP and laponite, respectively). Accordingly, the total mass of water (m_w) was established considering both the distilled water added into the mixtures and the initial SPP and laponite moisture content values. The mass values of SPP and laponite in solution were normalized as follows:

$$c_{SPP} = \frac{m_{SPP}}{m_w + m_{SPP} + m_{lap}}.100 \quad (3)$$

$$c_{lap} = \frac{m_{lap}}{m_w + m_{SPP} + m_{lap}}.100 \quad (4)$$

where:

c_{SPP} = rheological additive dosage, %,
c_{lap} = laponite content, %,
m_w = total mass of water, g,

FIG. 2

Mixing system: (*A*) overhead mixer; (*B*) detail of impeller; and (*C*) detail of tank dimensions.

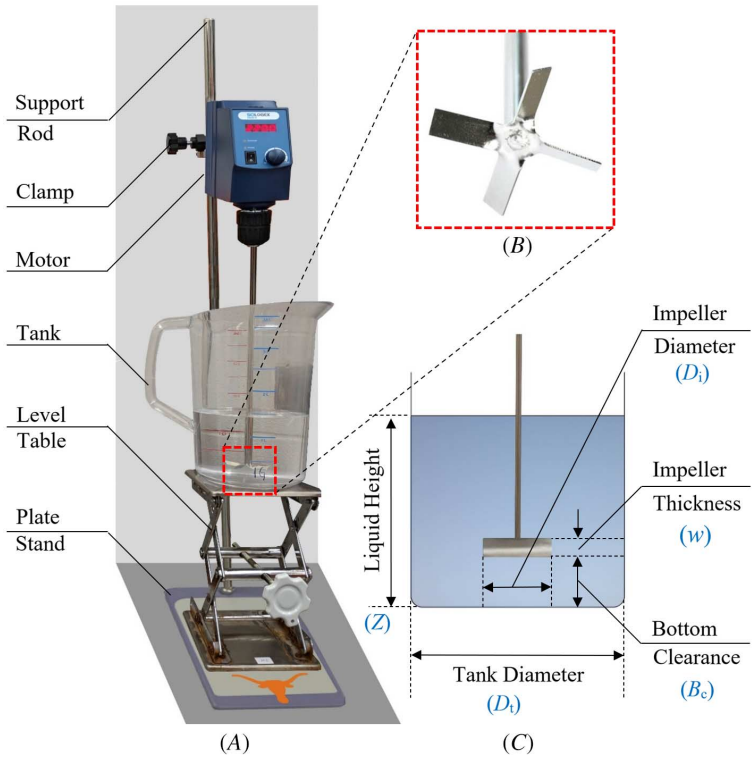

m_{SPP} = oven-dried mass of SPP, g, and

m_{lap} = oven-dried mass of laponite, g.

The overhead mixer was set to a relatively high rate of rotation (2,200 rpm) to facilitate laponite hydration and mixture homogeneity. It should be noted that the chemicals were added to the solution in air-dried conditions. The batches of laponite slurry prepared in each stage had an average volume of 1.5 L, with mixing being conducted for approximately 10 min. The SPP dosage and laponite content ranged from 0.00 % to 3.28 % and from 1.89 % to 11.33 %, respectively.

Samples were molded immediately after mixing to minimize the influence of aging. The slurry was poured into recipients or molds, depending on the laboratory tests to be carried out, for predefined aging periods (0.25, 1, 7, 14, and 28 days) at a constant laboratory air temperature (20°C). Individual samples were covered with a polyethylene plastic film to minimize desiccation and evaporation before testing.

Remixing

The "house of cards" structure (fig. 1C) that characterizes laponite in hydrated form is partly lost when the sample is subjected to shearing. However, the thixotropic nature of laponite tends to reestablish the original structure after shearing ceases with increasing aging time. This response is particularly useful when considering the reuse of laponite samples after testing. Even though this self-healing capability may facilitate the reuse of previously tested samples, the impact of remixing on transparency required proper evaluation of the material obtained after implementing this procedure.

The remixing procedure adopted in this study entailed the following steps: (1) pouring a thin layer with 10-mm depth of laponite aqueous solution on top of the laponite sample to be remixed (using the same laponite content and SPP dosage); (2) carefully introducing the impeller into the hydrated gel; (3) setting the overhead mixer to a target mixing speed (60 rpm, or 240 rpm) that was considerably lower than the original mixing speed (2,200 rpm) to

minimize the formation of air pockets; and (4) carefully maneuvering the impeller within the sample, ensuring adequate remixing of the original material. Following remixing, samples remained covered with a polyethylene plastic sheet until testing to avoid the development of superficial cracks (desiccation) and accumulation of impurities.

In this paper, the term "laponite sample" is used to refer to initial samples prepared by mixing laponite powder into a solution of water and additive (i.e., first-time hydrated samples). Instead, the term "remolded sample" is adopted to refer to a previously hydrated sample subjected to remixing.

OPTICAL AND PHYSICAL PROPERTIES

The optical and physical properties of laponite, in hydrated and powder forms, are discussed in this section.

Microstructure and Fabric

Light microscopy was used to evaluate inclusions that had been identified in the laponite microstructure (using an Axiovert 200M Fluorescent Microscope manufactured by Zeiss). Samples of hydrated laponite prepared with various laponite contents, and additive dosages were placed in special glass chambers tailored for these tests. Laponite samples in hydrated and powder forms were also evaluated using scanning electron microscopy (SEM) using a Zeiss Supra 40V Scanning Electron Microscope. An ultrathin layer of conductive paint (platinum/palladium coat 15-nm thick) was applied over dried samples before SEM analysis to enhance conductivity. **Figure 3** presents light microscopy and SEM test results, which are discussed next.

Figure 3*A* shows inclusions that were identified using light microscopy techniques (including unhydrated laponite stacks, impurities, and air pockets), also indicating the additive mass ratio (*AMR*) associated with each sample. The *AMR* is obtained as the ratio between the mass of additive and laponite (m_{SPP}/m_{lap}). The presence of unhydrated laponite crystals revealed that a fraction of laponite crystals did not disperse in water, possibly creating a source of light scattering (Nicolai and Cocard 2000) that affects transparency. Filtration techniques have been adopted in previous studies to decrease the presence of impurities, also contributed to reducing the amount of unhydrated laponite crystals (e.g., Bonn et al. 1999; Nicolai and Cocard 2000), although the effect of filtration on transparency was not evaluated in such studies.

The *AMR* was identified as a useful index to normalize the behavior of laponite samples in this study. In fact, it was possible to correlate insufficient additive dosage with the presence of air pockets within the hydrated laponite microstructure based on images collected by light microscopy. The software ImageJ was used to collect information on the size and frequency of the air pockets, i.e., measurements of the average diameter of air pockets (D_{air}) found in different samples, as shown in **figure 3*A***.

Based on SEM analysis test results, **figure 3*B*** shows the surface morphology of oven-dried hydrated laponite as well as a closer view revealing the superficial cracks resulting from volumetric shrinkage. The development of shrinkage cracks is related to the chemical dissociation that occurs when laponite meets atmospheric carbon dioxide (Ruzicka, Zulian, and Ruocco 2006), as previously discussed in this paper. Accordingly, laponite has the capability of returning to the original structure when water is readily available because the thixotropic nature of laponite allows it to reestablish its original structure, possibly supporting sample reuse.

The fabric of laponite powder is shown in **figure 3*C***. The figure illustrates several aggregations of structural units or laponite crystals. Images collected during SEM analysis were used to assess the apparent particle size distribution and other shape characteristics of the laponite crystals. The software ImageJ was used to collect the parameters such as the diameters of the largest and smallest circles (D_{max}, and D_{min}, respectively) that fit into the identified laponite crystals. The representative diameter (D_R) of each crystal was defined as follows:

$$D_R = \frac{D_{min} + D_{max}}{2} \tag{5}$$

where:

D_{min} = minimum diameter, μm,
D_{max} = maximum diameter, μm, and
D_R = representative diameter, μm.

FIG. 3

Light microscopy and SEM results: (*A*) microstructure of hydrated samples; (*B*) fabric of oven-dried hydrated laponite; and (*C*) View of laponite powder particles.

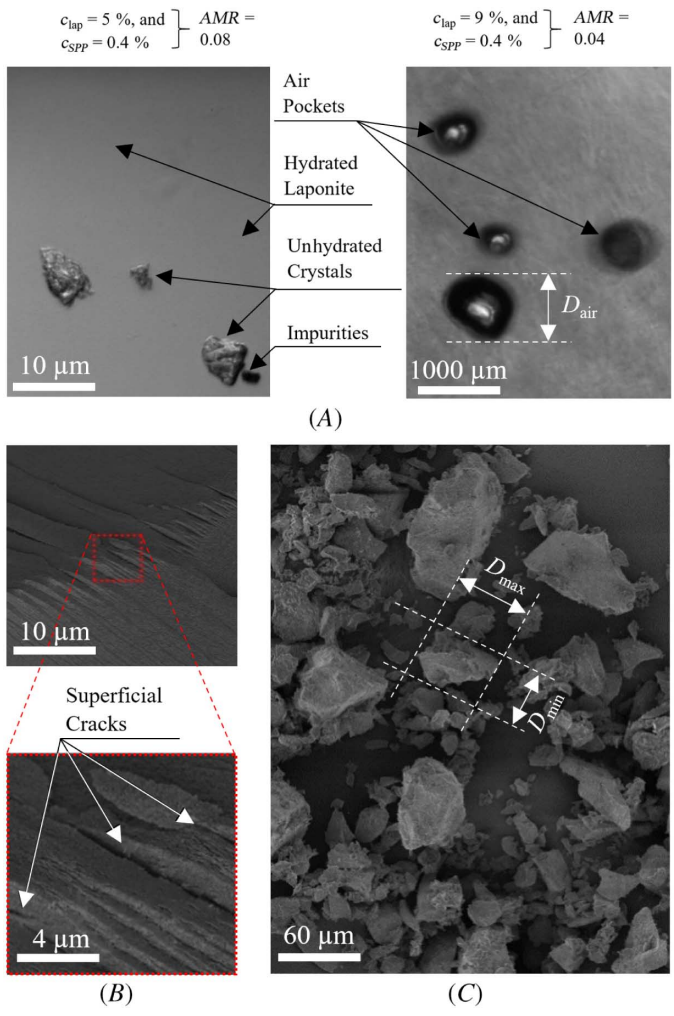

Figure 4A presents the average diameter of air pockets observed in samples prepared using increasing values of laponite content and different additive dosages (shown in the figure as *AMR*). The results in **figure 4A** show that, for a given laponite content, the diameter of air pockets correlates well highly with the additive dosage. The diameter of air pockets in samples for a given *AMR* was found to increase exponentially with increasing laponite contents. The trend of the experimental data could be represented as follows:

$$D_{air} = \exp(k_1 + k_2 \times \sqrt{c_{lap}}) \quad (6)$$

where:

D_{air} = diameter of the air pockets, mm, and

k_1 and k_2 = constants, dimensionless.

Coefficient k_1, as expressed in equation (6), could be assumed to have a constant value of (−7) regardless of additive dosage and laponite content. On the other hand, coefficient k_2 showed values of 3.33, 2.57, 2.04, 1.99, and 1.90 for *AMR* of 0, 0.01, 0.04, 0.14, and 0.27, respectively. Based on these results, laponite contents up to 4 % provided adequate levels of workability associated with *AMR* above 0.01, whereas laponite content exceeding 4 %

FIG. 4 Properties associated with light microscopy and SEM results: (*A*) effect of *AMR* on air pocket diameter; and (*B*) particle size distribution of laponite powder and unhydrated particles.

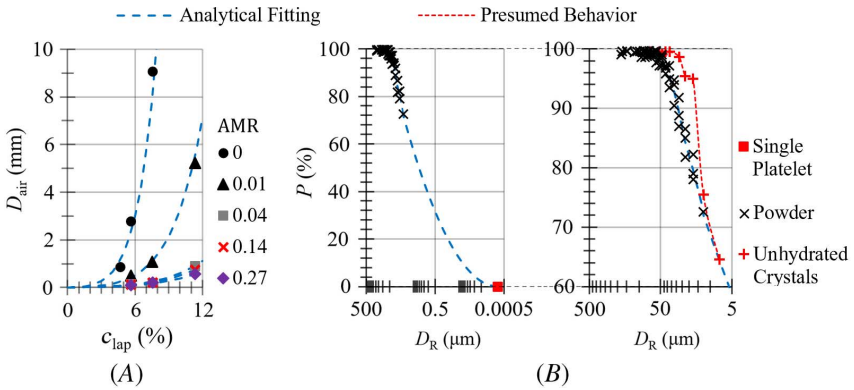

required larger amounts of additive to improve workability. Considering the observed relationships among laponite contents, *AMR*, and workability, an optimum additive dosage was identified for different laponite contents, which led to enhanced OC (see next section of this paper).

Analysis of SEM images allowed evaluation of the particle size distribution of laponite powder crystals and unhydrated crystals, as depicted in figure 4*B*. The single platelet size shown in this figure is associated with the dimensions of a microscopic single laponite platelet, reported as 25 nm by Ruzicka and Zaccarelli (2011). An exponential function was found to fit well ($R^2 > 95$ %, with R^2 representing the coefficient of determination) with data collected on laponite powder's particle size distribution, according to the following function:

$$P = \exp(-6.97 + 1.12\sqrt{D_R}) \tag{7}$$

where:

P = percentage of particles finer than a certain diameter, %, and

D_R = representative diameter, μm.

Based on equation (7), 95 % of laponite powder crystals have a representative diameter smaller than 37.5 μm, whereas 95% of the unhydrated laponite crystals randomly distributed in the internal structure have an average diameter smaller than 17.5 μm. This reveals that sample preparation methods could be improved further (e.g., using filtration) to prevent the presence of unhydrated crystals due to deficient additive dosage.

Absorbance and Transmittance

High-resolution spectroscopy was conducted on laponite samples using a Cary 5000 high-performance Spectrophotometer, which works in the 220–800-nm wavelength range and can independently measure the absorbance and transmittance spectra. A sample with 5 % laponite content and 0.4 % SPP dosage was selected, considering that these dosages resulted in air pockets of comparatively smaller diameters (fig. 4*A*). Figure 5 presents the spectroscopy test results.

Figure 5*A* presents the resulting transmittance and absorbance spectra for the sample containing 5 % laponite content and 0.4 % SPP dosage. Transmittance levels exceeding 81.85 % were observed for wavelengths corresponding to the spectrum of visible light (390 nm [violet] to 780 nm [red]) associated with a path length of 10 mm. Maximum transmittance levels were found to correspond to wavelengths ranging from 628 nm to 717 nm (88 % to 90 % transmittance, respectively), which corresponds to the red-light spectra (622–780 nm, as in Hecht 2017). Absorbance levels of 0.05110 were detected for the same wavelength range.

FIG. 5

Spectroscopy results of a sample with a laponite content of 5 % and SPP dosage of 0.4 %: (*A*) transmittance and absorbance spectra; (*B*) illustration of testing setup; and (*C*) comparison between gauge readings and tracked displacements for a sample with 100-mm depth.

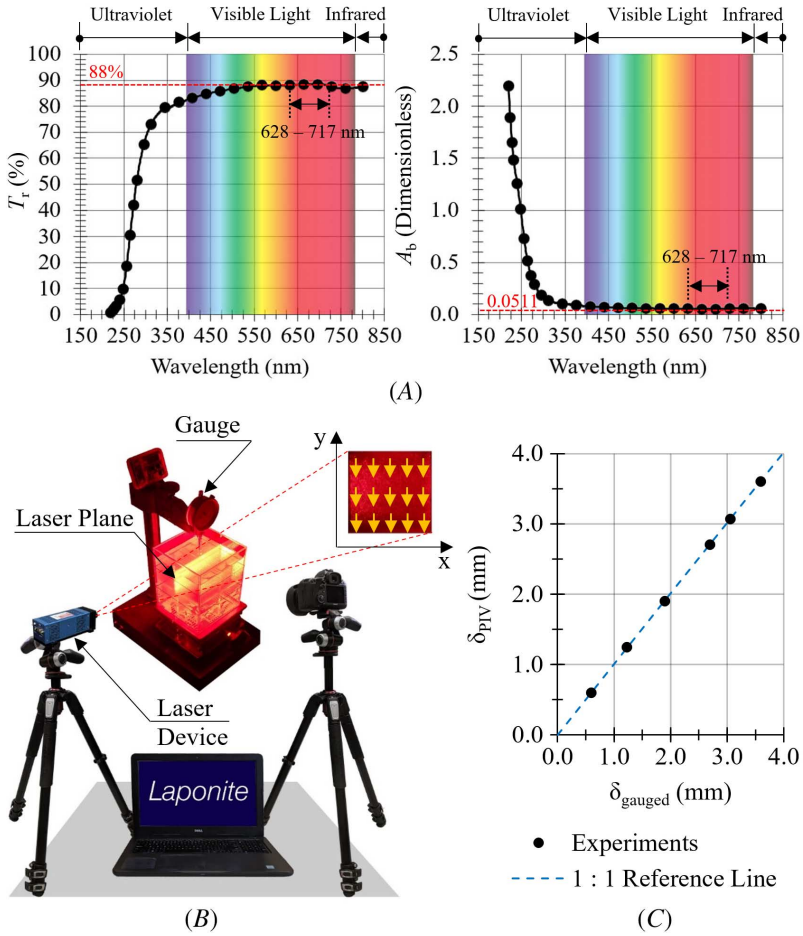

It should be noted that the absorbance of a beam of collimated monochromatic radiation in a homogeneous isotropic media can be quantified by the Beer–Lambert law when it adheres to the following relationship:

$$A_b = \varepsilon.c_m.l = \log(1/T_r) \tag{8}$$

where:

A_b = absorbance, dimensionless,
ε = molar absorptivity coefficient, $L \times mol^{-1} \times cm^{-1}$,
c_m = molar solute concentration, mol/L,
l = optical path length, cm, and
T_r = transmittance, %.

Because absorbance and transmittance spectra were measured independently, it was possible to correlate experimental results and values predicted according to equation (8). The calculated absorbance spectra correlated strongly ($R^2 > 99$ %) with the real values measured during testing, indicating that the tested sample of hydrated laponite followed the Beer–Lambert law. Negligible diffuse reflectance was measured by the specific module coupled to the spectrophotometer, providing evidence that absorbance was the most relevant factor affecting the transparency of the tested laponite sample for an optical path length of 10 mm.

Considering that both the optical path length ($l = 10$ mm) and the molar absorptivity coefficient (ε) are constants (equation (8)) during testing, the absorbance of hydrated laponite is primarily dependent on the

concentration of this chemical compound in solution. Thus, it can be concluded that both absorbance and transmittance are dependent on laponite concentration, which ultimately impacts the resulting OC.

Laser Penetration Depth

Laser technology has been used to enhance experimental capabilities by highlighting particle positions in geotechnical physical models involving transparent soil (e.g., Iskander 2010). However, their use may be limited by the depth of laser penetration into laponite samples. The percentage of absorption is related to the decay of light intensity with depth at a rate determined by the absorption coefficient, which is a function of the wavelength and temperature (Brown and Arnold 2010). The optical penetration or absorption depth for materials that follow the Beer–Lambert law is defined as follows:

$$\delta = 1/k_{\mathrm{A}} \tag{9}$$

$$k_{\mathrm{A}} = \frac{1}{l}.\ln\frac{[1-(R/100)]^2}{T_{\mathrm{r}}/100} \tag{10}$$

where:

δ = laser penetration depth, cm,
k_{A} = absorption coefficient, cm^{-1},
l = optical path length, cm,
R = reflectance, %, and
T_{r} = transmittance, %.

A laser diode module from Coherent, model PL-501, was selected for this study. This device works at a wavelength of 670 nm (±10 nm of tolerance), has a power rating of 500 mW, and a fan angle of 30°. Under these conditions and considering the transmittance spectra (**fig. 5*A***), hydrated laponite (6 % laponite and 0.06 % SPP) presents 88.24 % transmittance and k_{A} of 0.125 cm^{-1} (equation (10)) at an air temperature of 20°C. This leads to a penetration depth of 80 mm (equation (9)). However, this estimate may not define the penetration depth accurately, as penetration depth is also a function of factors that are not considered in equation (9).

Given the uncertainties related to the range of laser penetration depth within laponite and therefore possible inaccuracy in collected data, additional testing was performed to quantify the magnitude of errors related to displacement estimates. A selected sample of hydrated laponite (5 % laponite and 0.4 % SPP dosage) was placed into an acrylic container with a square footprint of a 127-mm side length and a height of 100 mm, as shown in the testing setup represented in **figure 5*B***. A camera was positioned perpendicular to the reference vertical plane located within the transparent soil sample. The computer-controlled camera was programmed to capture images after each increment of vertical displacement, facilitating the assessment of the resulting displacement fields.

The reference plane consisted of a thin vertical layer (approximately 10 mm) of a mixture prepared with 5 % laponite and 0.05 % SPP, which was strategically positioned at the middle length of the box to produce a speckle pattern under laser illumination. Air pockets are inherent to this laponite content and *AMR* (equation (5)), thus serving as seeding particles in this test. The MATLAB subroutine developed by Blair and Dufresne (2008) was used to identify the position of the air pockets captured in each picture, supporting the determination of the fields of displacements based on a sequence of pictures.

The accuracy of displacement measurements was quantified by the percent error defined as the following:

$$E = \frac{\delta_{\mathrm{gauged}} - \delta_{\mathrm{PIV}}}{\delta_{\mathrm{PIV}}}.100 \tag{11}$$

where:

E = error, %,
δ_{gauged} = gauged displacement, mm, and
δ_{PIV} = tracked displacement, mm.

Figure 5C shows a comparison between gauge readings and tracked displacements, providing insight into the average magnitude of the errors associated with the testing procedures. The average percent error (equation (11)) of these tests was 0.33 %, showing that good agreement could be achieved between the experimental data and tracked displacements.

Refraction

The refractive index of isotropic media is governed by the Lorentz–Lorentz Formula (Lorentz 2004), which relates the refractive index of a substance to its density, absolute temperature, and wavelength. Based on the studies of Lorentz (2004), the following equation can be used to describe the refractive index of a transparent medium (Schiebener and Straub 1990) for a constant wavelength:

$$\frac{n_D^2 - 1}{n_D^2 + 2} \cdot \frac{1}{\rho} = \alpha_0 + \alpha_1 . \rho + \alpha_2 . T_m \tag{12}$$

where:

n_D = refractive index of the sample at the reference D-line, dimensionless,
ρ = specific gravity of the solution, g/cm^3,
α_0, α_1, and α_2 = fitted coefficients, dimensionless, and
T_m = absolute temperature, K.

The refractive index of hydrated laponite samples was assessed using a digital refractometer that operates at a constant wavelength of 589.3 nm. Refractive indexes were measured at aging times of 1, 7, 14, and 28 days at an air temperature of 20°C. Samples involved laponite contents ranging from 3 % to 11 %, with and without rheological additive. Test results were evaluated considering a constant wavelength as indicated in equation (12) by plotting a graph of $(n_D^2 - 1)/(\rho.(n_D^2 + 2))$ in relation to ρ under constant air temperature (i.e., Schiebener and Straub 1990; Kumar et al. 2008). The results are plotted in figure 6, with figure 6A showing results obtained using samples with no rheological additive and figure 6B considering results obtained using samples with 0.4 % SPP dosage.

When considering the solutions with no rheological additive (fig. 6A), the fitted linear trend involves a coefficient α_1 of −0.1484, and an intercept $(\alpha_0 + \alpha_2.T_m)$ of 0.3534. When a 0.4 % SPP dosage was used (fig. 6B), coefficient α_1 is −0.1376, and the intercept $(\alpha_0 + \alpha_2.T_m)$ is 0.3424. It was not possible to differentiate coefficients α_0 and α_2, as tests were conducted at a constant temperature (20°C). Even in the absence of such

FIG. 6 Refractive indexes at 20°C fitted to the extended Lorentz–Lorentz equation: (*A*) no rheological additive and (*B*) rheological additive at a dosage of 0.4 %.

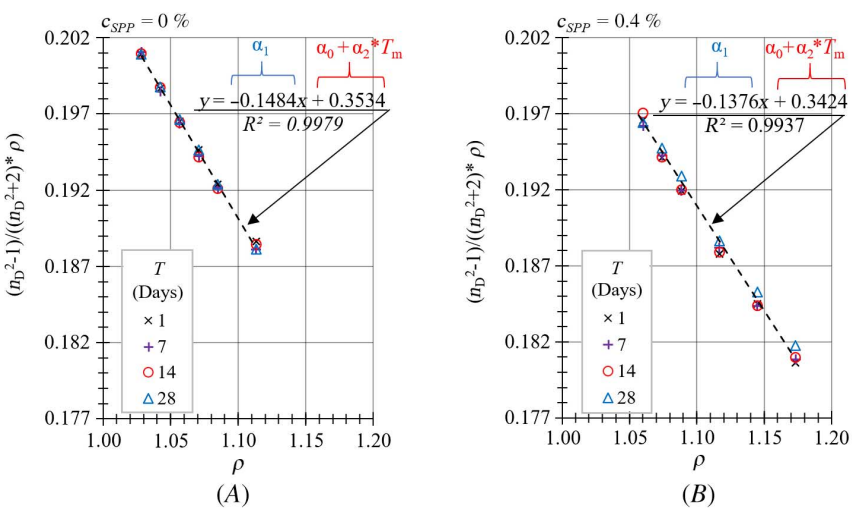

information, experimental data clearly show a trend consistent with the findings reported by Kumar et al. (2008), which proposed a coefficient α_1 of −0.13 and an intercept ($\alpha_0 + \alpha_2.T_m$) of 0.3592 for laponite content ranging from 2 % to 3.5 % and no additives, at a temperature of 20°C.

For samples with no rheological additive (**fig. 6*A***), the refractive index ranged from 1.3346 (2 % laponite) to 1.3407 (8 % laponite). These values are in line with those reported by Kumar et al. (2008), who reported refractive index values ranging from 1.3345 to 1.3365 for laponite contents ranging from 2.0 % to 3.5 %. Accordingly, for samples with an SPP dosage of 0.4 % (**fig. 6*B***), the refractive index ranged from 1.3372 to 1.3466. Given the agreement with the Lorentz–Lorentz formula (equation (12)), it may be concluded that density represented the most significant factor affecting the refractive index of hydrated laponite, aside from the anticipated influence of temperature. Because laponite concentration and additive dosage are the most relevant factors impacting the density of the sample at a constant air temperature, both laponite concentration and additive dosage had a major influence on the resulting refractive index values. On the other hand, aging time exhibited no relevant effect on the refractive index of hydrated laponite.

Assessment of Transparency

The testing setup used in this research component is illustrated in **figure 7*A***. Laponite in its initial liquid form was poured into the acrylic containers to reach the required depth of visualization. These acrylic containers had internal dimensions of 127 mm in length and width and allowed depths of visualization of 100, 300, and 600 mm. Samples were stored and coved by polyethylene film during predefined aging periods (0.25, 1, 7, 14, and 28 days)

FIG. 7

OC results of samples tested using 100-mm depth: (*A*) image analysis testing setup; (*B*) samples without additives; (*C*) selected samples with rheological additives; and (*D*) changes in OC for different *AMR*.

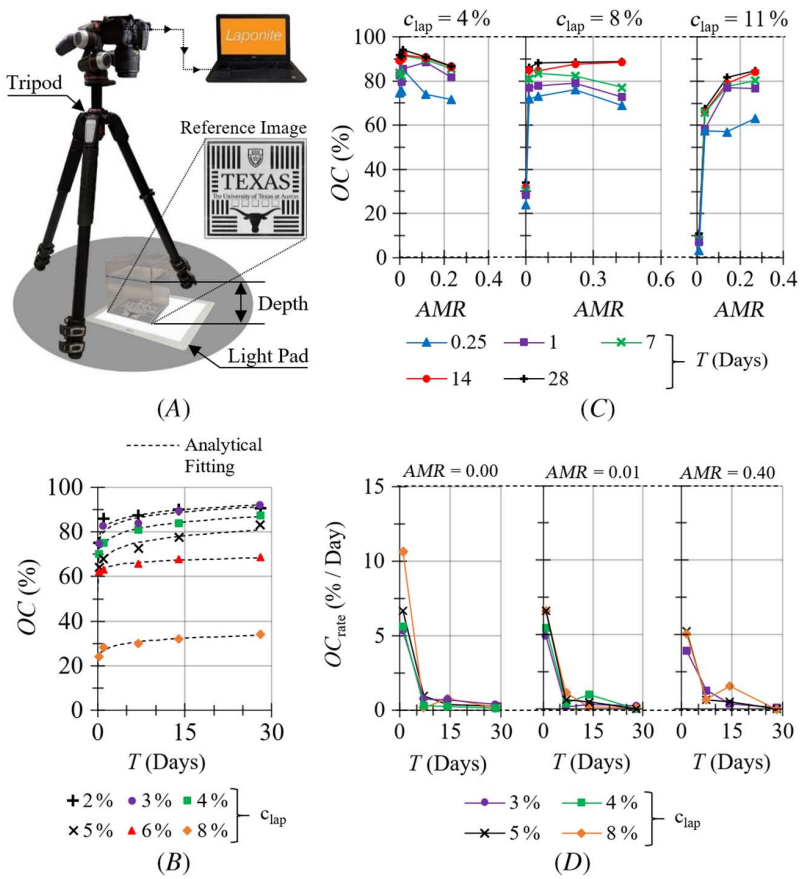

at a temperature of 20°C. Before testing, samples were placed over a light pad, which served as a luminous background for enhanced picture collection.

A reference image consisting of black and white stripes and additional shapes with defined edges was placed over the light pad to enhance image quality by inhibiting variations in shades and bright areas. A Nikon D5500 Digital Single Lens Reflex (DSLR) camera with an 18-55 mm lens was used. Camera parameters were fixed at a focal length of 55 mm, aperture of f14, shutter speed of 1/10th s (depths of visualization of 100 and 300 mm) or 1/4th s (depth of visualization of 600 mm), ISO of 100, auto white balance, and no flash.

Two-dimensional linear image correlation was used to assess differences in OC between images. The correlation coefficient (R) has a value of 1 if a pair images are identical and a value of 0 if no correlation exists. The correlation R between a reference image "X" and a given image captured during testing "Y" can be calculated from pixel intensity array subsets of a pair of images with identical size, as follows (e.g., Spiegel and Stephens 2011):

$$R = \frac{\Sigma_m \Sigma_n [(X_{mn} - \bar{X}).(Y_{mn} - \bar{Y})]}{\sqrt{[\Sigma_m \Sigma_n (X_{mn} - \overline{\bar{X}})^2].[\Sigma_m \Sigma_n (Y_{mn} - \overline{\bar{Y}})^2]}} \quad (13)$$

where:

R = correlation coefficient, dimensionless,
m = row pixel location, dimensionless,
n = column pixel location, dimensionless,
$\bar{X}$ = mean intensity value of matrix X, dimensionless, and
$\bar{Y}$ = mean intensity value of matrix Y, dimensionless.

A MATLAB subroutine was developed for the analysis of the images collected in this study. Image preprocessing involved converting the original Red, Green, and Blue (RGB) pictures to grayscale by eliminating the hue and saturation information while keeping the same luminance. Intensity values at a certain pixel location ranged from 0 (black) to 255 (white) in grayscale pictures. Image alignment and cropping were performed to ensure analysis of the same area in both pictures, along with the same picture resolution. When comparing the reference image with a sample of hydrated laponite, the coefficient of linear correlation was in the range of $0 \leq R \leq 1$, serving as a quantitative indicator of the transparency, i.e., OC ranging from 0 % ($R = 0$) to 100 % ($R = 1$).

EFFECT OF RHEOLOGICAL ADDITIVE DOSAGE, LAPONITE CONTENT AND AGING TIME

The effects of laponite content and aging time on OC are represented in **figure 7*B***, for samples with increasing laponite content and no rheological additives. The overall trend shows an increasing OC with increasing aging time and decreasing laponite content. A marked decrease in transparency was observed for samples with laponite content above 5 % when no additive was added, a trend that can be attributed to incomplete mixing when using comparatively high laponite dosages. Essentially, the absence of additive in solution resulted in increasing stiffness during mixing, which translated into poor workability. Such poor workability in the early stages of the mixing process resulted in trapped air pockets and contributed to a decreased OC. The data fitting shown in **figure 7*B*** is further discussed in later sections of the paper.

Figure 7*C* presents the effect of the rheological additive on the OC of samples prepared with laponite contents of 4 %, 8 %, and 11 % at different additive dosages and aging periods. Similar trends were observed for samples with laponite contents of 5 % and 6 %, which are omitted for conciseness. It was not possible to determine optimum *AMR* for laponite contents of 2 % and 3 % because of the lack of a structured internal particle arrangement (e.g., Ruzicka and Zaccarelli 2011) associated with low laponite contents (less than 4.0 %). However, these materials may have limited use as surrogates of natural clays in geotechnical models regardless of the additive dosage.

As shown by the results in **figure 7*C***, the use of rheological additive facilitated mixing considerably, thus improving the OC of samples in relation to samples with no additives, in agreement with the findings of Beemer

et al. (2016). The data displayed in this figure substantiate the existence of an additive mass rate that optimizes OC. Specifically, the trends show an increase in OC up to a certain dosage of rheological additive, i.e., *AMR* of 0.015, 0.08, 0.09, 0.2, and 0.27 for laponite contents of 4 %, 5 %, 6 %, 8 %, and 11 %, respectively.

The transition in behavior associated with optimum *AMR* is particularly relevant from a geotechnical modeling perspective, given the considerable effect of additives on transparency and the anticipated effect on geotechnical properties. The following equation was found to be representative of experimental data ($R^2 = 95$ %), serving to represent the relation between optimum *AMR* and the laponite content:

$$AMR_{\text{opt}} = b_1 + b_2/c_{\text{lap}} \tag{14}$$

where:

AMR_{opt} = optimum *AMR*, dimensionless, and

b_1 and b_2 = fitted coefficients, dimensionless.

The values assumed by the fitted coefficients b_1 and b_2, as indicated in equation (14), were 0.3983 and −1.50976, respectively. Accordingly, equation (14) is valid for laponite contents equal to or larger than 4 %. It should be noted that these values are associated with the testing conditions adopted in this research, i.e., mixing apparatus and procedures, laboratory air temperature, and chemical components.

Considering the relevant influence of aging on transparency, an additional evaluation was conducted to investigate the mechanisms influencing the progressive increase of OC with sample aging. For the purposes of this evaluation, a transparent soil sample was considered to have aged 0 days (t_0) right after sample preparation. A reference picture captured from the same sample aged "t_1" days allowed calculation of the correlated OC, OC_{t_1}, and a second picture capture from the same sample aged "t_2" days led to calculated OC, OC_{t_2}. Considering that $t_2 > t_1$, the rate of change in OC between samples (2) and (1) was quantified as follows:

$$OC_{\text{rate}} = \frac{\Delta OC}{\Delta t} = \frac{OC_{t_2} - OC_{t_1}}{t_2 - t_1} \tag{15}$$

where:

ΔOC = change in OC, %,

OC_{rate} = rate of change in OC, %/day,

OC_{t_1} = OC for sample aged t_1, %,

OC_{t_2} = OC for sample aged t_2, %,

Δt = elapsed time between readings, day, and

t_1, and t_2 = age of a sample, day.

Considering that the OC was determined for samples aged 0.25, 1, 7, 14, and 28 days, **figure 7*D*** presents the rates of change in OC associated with the elapsed times between readings. *AMR* equal to 0.00, 0.01, and 0.40 were used in this analysis.

When considering samples with no additive, the highest rates of change in OC (**fig. 7*D***) corresponded to the mixture with a laponite content of 8 % and no additives (11 % improvement per day in early stages), whereas the other samples showed rates of change in OC ranging from 5 % to 7 % per day in early stages. In contrast, rates of change in OC declined substantially for samples aged 7 or more days (up to 1 % improvement per day) for samples with no additives. Similar trends were observed for samples containing rheological additives, indicating that most of the improvement in OC occurs in the early aging stages (up to 7 days). The large increase in OC after the initial mixing can be attributed to hydration reactions that occur within a few hours after initial mixing. Nonetheless, OC continues to increase after the laponite became fully hydrated. This time-dependent improvement in transparency after hydration can be largely related to the thixotropic behavior of laponite.

Overall, the results on OC (**fig. 7**) show that (1) aging time, laponite content, and additive dosage play important roles in OC because of hydration and the impact of aging; (2) increasing laponite content results

in a decreasing OC, a trend that is consistent with an increasing absorbance with laponite content, as well as with the presence secondary inclusions in the internal structure; and (3) increasing additive dosage leads to increasing OC but only up to an optimum content, beyond which a decrease in OC is observed due to delayed aging. These results provide the basis to predict OC of aged samples, based on laponite content and *AMR*, discussed as follows.

PREDICTION OF OC

An exponential function was fitted to experimental data representing the relationship between laponite content, aging time, and *AMR*. The function shows a strong correlation with the experimental data ($R^2 > 90$ %) and can be represented as follows:

$$OC = L_1 . T^{L_2} \tag{16}$$

where:

L_1 and L_2 = fitted coefficients, dimensionless, and

T = aging time, days.

Dimensionless coefficient L_1 expresses the OC in the early stages after mixing because it is not dependent on the aging time in equation (16). The following equation was found to be representative of experimental data ($R^2 > 90$ %), serving to represent the relation between coefficient L_1 and the laponite content:

$$L_1 = (p_1 + p_2 . c_{lap}^2)^2 \tag{17}$$

where p_1 and p_2 = fitted coefficients, dimensionless.

On the other hand, fitting coefficient L_2 incorporates the effect of aging on OC. The following function was found to strongly correlate with the experimental data ($R^2 > 90$ %):

$$L_2 = q_1 . c_{lap}^{q_2} \tag{18}$$

where q_1 and q_2 = fitted coefficients, dimensionless.

Figure 8 represents the values of the dimensionless coefficients, i.e., (*A*) L_1, and L_2, and (*B*) p_1, p_2, q_1, and q_2, for different laponite contents and additive mass rates.

FIG. 8

Dimensionless coefficients used to predict the OC of aged samples depending on the laponite content and *AMR*, as obtained using laponite samples with 100-mm depth: (*A*) parameters L_1 and L_2; and (*B*) parameters p_1, p_2, q_1, and q_2.

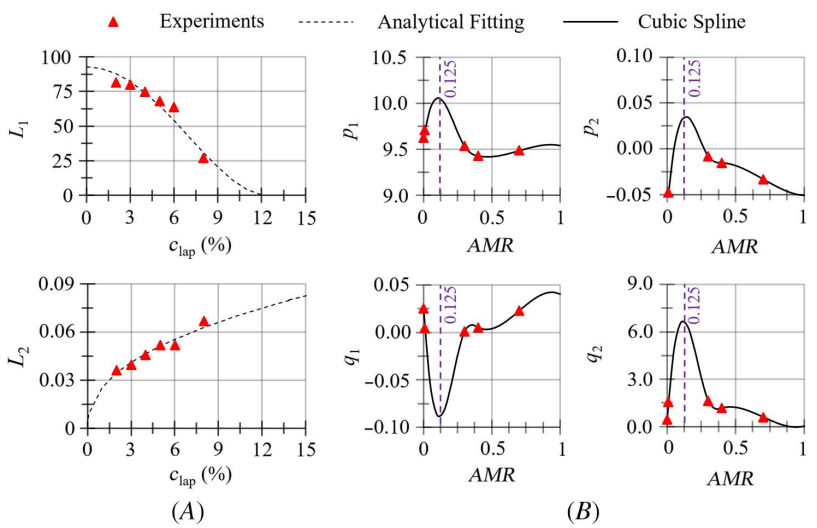

As figure 8B shows, cubic spline curves were fitted to represent the experimental data representing coefficients p_1, p_2, q_1, and q_2. Maximum and minimum values for these coefficients can be defined when plotted against the *AMR*, with all of them showing the maximum/minimum for a value of *AMR* of approximately 0.125, which appears to be associated with a transition from deficient to excessive additive dosages.

Figure 9A depicts the contour curves associated with parameters L_1 and L_2 for different laponite content and *AMR*. Parameter L_1, which represents the OC in early stages of aging after mixing following hydration, ranged from 20 to 90, whereas parameter L_2, which accounts for the effect of time on OC related to thixotropy gains, ranged from 0.01 to 0.1. Parameters L_1 and L_2 presented opposite trends, denoting that although samples with lower laponite concentrations are prone to present higher OC in early stages, the effect of aging is more pronounced by samples with higher laponite contents. This trend is also consistent with the results presented in figure 8A.

Figure 9B depicts the combined effects of dimensionless parameters on OC of samples with 100 mm of depth. A progressive increase in OC with aging time is evident, which is also impacted by the laponite content and *AMR*.

FIG. 9

Effect of rheological additive on OC of samples with 100 mm depth: (*A*) fitted parameters L_1 and L_2, and (*B*) OC for samples aged.

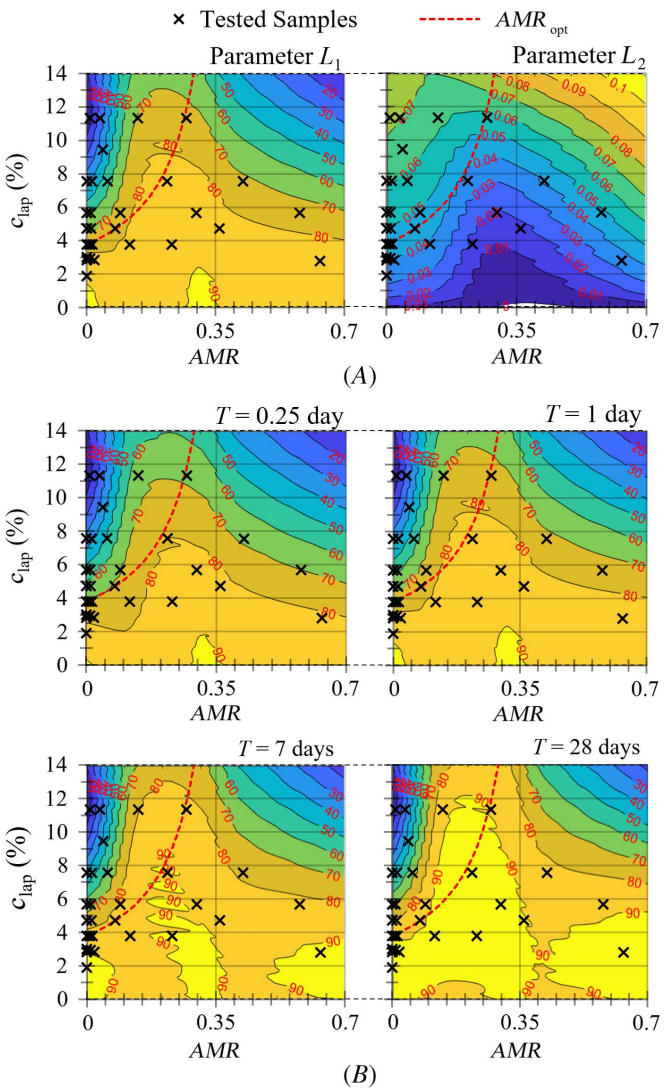

EFFECT OF DEPTH OF VIEWING PLANE

This section discusses the effect of depth of viewing plane on OC, followed by the quantification of its impact on the accuracy of displacement tracking.

Results as summarized in **figure 10**, with **figure 10*A*** indicating the relation between OC, depth of viewing plane (100, 300, and 600 mm), laponite content (ranging from 4 % to 11 %), and aging, considering a constant additive dosage (0.4 %). The optimum *AMR* (equation (14)) associated with laponite contents of 4 %, 5 %, 6 %, 8 %, and 11 % are 0.021, 0.096, 0.147, 0.210, and 0.261, and tested *AMR* (**fig. 10*A***) corresponded to 0.1, 0.08, 0.070, 0.05, and 0.040. Thus, samples with a laponite dosage of 4 % and 5 % roughly match the optimum *AMR*, and samples with a laponite dosage of 6 %, 8 %, and 11 % laponite correspond to additive under dosage. The poor workability resulting from deficient additive content for samples containing 6 %, 8 %, and 11 % laponite resulted in trapped air pockets, which led to a decreased OC. On the other hand, samples with adequate additive dosage (4 % and 5 % laponite) showed relatively high OC for depths of the viewing plane ranging from 100 to 600 mm.

Overall, the following observations can be drawn from the experimental results (**fig. 10*A***): (1) OC increases with decreasing depths of viewing plane, decreasing laponite contents, and increasing aging time; (2) a significant drop in OC occurs when the additive dosage is insufficient to allow adequate mixing of the solution (samples containing 6 %,

FIG. 10 Effect of depth on OC: (*A*) effect of laponite contents and aging times; (*B*) testing setup for image analysis; and (*C*) comparison between gauged readings and tracked displacements for a sample with a laponite content of 5 % laponite and SPP dosage of 0.4 %.

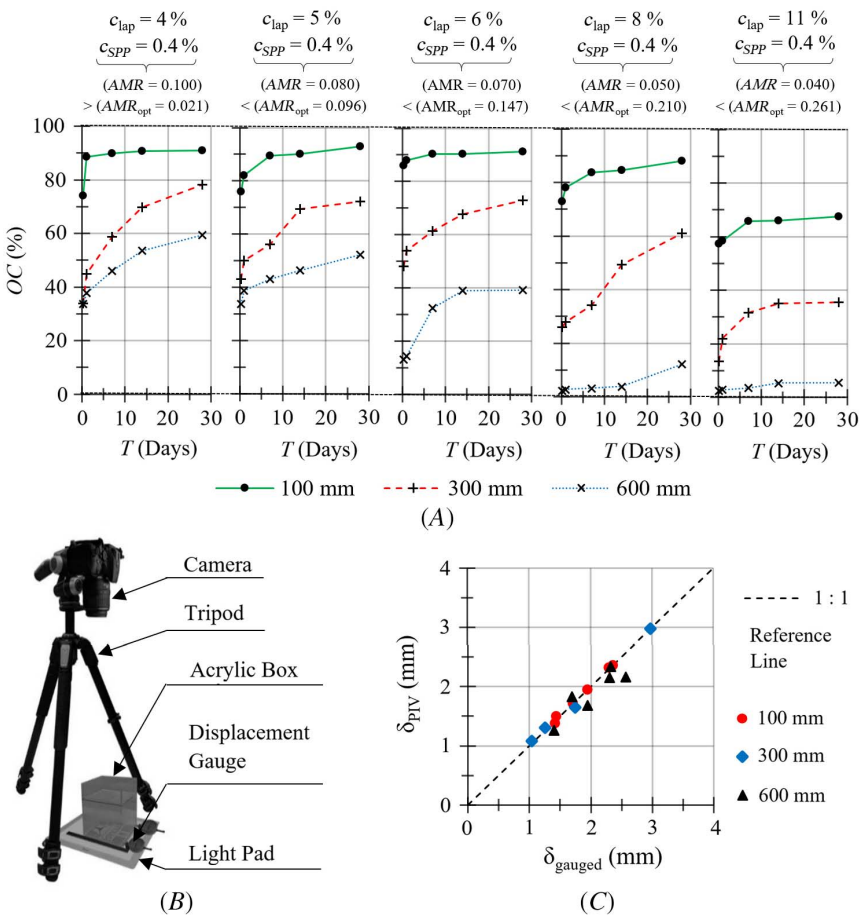

8 % and 11 % laponite); and (3) secondary elements found in the internal structure, such as impurities, unhydrated laponite stacks, and air pockets, have a greater effect on OC for comparatively large viewing plane depths.

Considering the good transparency for larger depths of visualization of samples with adequate additive dosage, a sample containing 5 % laponite and 0.4 % SPP dosage and aged 7 days was used to assess the accuracy of displacement tracking methods for different depths of the viewing plane (100, 300, and 600 mm). The testing setup is shown in **figure 10*B***. A reference image was affixed to the bottom of the acrylic containers (similarly to **fig. 7*A***). The testing procedure involved moving the acrylic containers horizontally while monitoring gauged displacements and capturing pictures of the reference image following each step of horizontal displacement. Pictures were taken with the same resolution to facilitate testing accuracy. The Particle Image Velocimetry (PIV) technique was used to track the field of displacement vectors, following the MATLAB routine developed by Thielicke and Stamhuis (2014).

A comparison between gauged and tracked displacements is presented in **figure 10*C***. The percent error used to quantify the accuracy of displacements, calculated according to equation (11), resulting in errors of 0.28 %, 1.67 %, and 6.66 % for visualization depths of 100, 300, and 600 mm, respectively. Each testing phase consisted of applying incremental displacements on the order of 1 mm, resulting in a discrepancy between gauged and tracked displacements corresponding to 0.002, 0.017, and 0.0665 mm, for depths of visualization of 100, 300, and 600 mm, respectively. These results show that comparatively large test setups are a viable alternative for geotechnical physical models when dealing with adequate additive dosages, especially for relatively low laponite contents.

EFFECT OF SAMPLE REMIXING

Samples aged 28 days were subjected to remixing to allow evaluation of the viability of reusing laponite samples by quantifying its effect on transparency. The following procedure was adopted: (1) a thin layer of laponite in liquid form with approximately 10-mm depth was poured on top of samples with the same laponite content and additive dosage as the original sample; (2) this material was carefully remixed at different speeds (60 and 240 rpm) and left to rest; and (3) OC was determined for the aging times of 28.25, 29, 35, 42, and 56 days. **Figure 11** shows the results of these tests, obtained after remixing at speeds of (*A*) 60 rpm and (*B*) 240 rpm.

A pronounced decrease in OC can be observed immediately after remixing (**fig. 11**), regardless of the laponite content and additive dosage. As previously discussed in this paper, hydrated laponite has the capability to reestablish the original structure after shearing with increasing aging time. This behavior was also associated with a progressive

FIG. 11 OC for aged samples with 100 mm depth after remixing using speeds of: (*A*) 60 rpm and (*B*) 240 rpm.

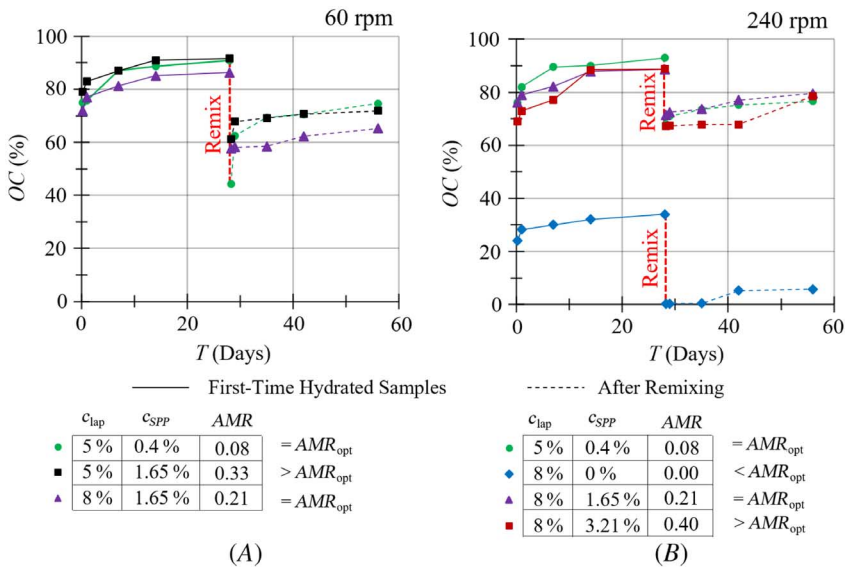

increase in OC with increasing aging time, despite the initial pronounced decrease. The changes in OC (ΔOC) between 28 days (first-time hydrated samples) and 56 days (remixed) samples were, on average, −20 % for samples remixed at 60 rpm, and −15 % for samples remixed at 240 rpm. Sample with a laponite content of 8 % and no additives resulted in comparatively poor OC due to trapped air pockets, indicating that additive dosage does not only improve the workability of first-time hydrated samples but also enhances the OC of remixed samples.

Based on the results of this evaluation, the following points can be highlighted: (1) optimum *AMR* was required to improve remixing capabilities; (2) remixing procedures must be meticulousness performed to avoid trapped air pockets, regardless of remixing speed rate; and (3) a pronounced decrease in OC is expected immediately after remixing, which is partially recovered with increasing aging time. Hydration reactions could ultimately be associated with the structural evolution of remixed hydrated laponite, contributing to the time-dependent OC behavior. This remixing procedure produced an essentially new sample taking advantage of the hydrated laponite capability to reestablish the original structure with increasing aging time.

Summary and Conclusion

This research focuses on generating experimental results to quantify the relevant factors that affect the transparency of laponite (Laponite-RD) for use as a clay surrogate in geotechnical physical modeling. An extensive testing program was conducted to obtain the optical and physical properties of laponite samples prepared under a wide range of conditions. The most relevant lessons learned are as follows:

- Aging time, laponite content, and dosage of rheological additive were found to be particularly relevant factors affecting transparency. Relationships were developed to allow the prediction of OC in terms of these factors.
- The *AMR* ($AMR = m_{SPP}/m_{lap}$) was found to be a key indicator of laponite transparency, as it strongly correlated with the workability and efficiency of laponite sample preparation procedures. Considering this parameter, values of optimum additive dosage could be defined for a specific laponite content.
- Changes in OC are particularly significant in the early aging stages after laponite sample preparation (from the initial mixing to 7 days [up to an 11 % increase]), which may be attributed to laponite hydration and early stages of aging. Aged samples presented a time-dependent increase in OC that averaged a 5 % increase over the subsequent 3 weeks.
- Relevant aspects of the time-dependent OC included quantification of maximum transmittance levels in laponite samples, which were observed for spectra of red light (transmittance of 88 % to 90 % for wavelengths ranging from 628 nm to 717 nm), and the refractive index of hydrated laponite, which was found to depend primarily on sample density and temperature.
- The reuse of laponite samples after remixing was evaluated and deemed feasible, which has important practical implications for large-scale testing setups. Samples must be prepared with optimum *AMR* to enhance remixing capabilities, and remixing procedures must avoid the trapping of air pockets. A decrease in OC may result upon remixing, but it was found to depend on the laponite content and additive dosage.

Overall, hydrated laponite was found to provide a viable modeling alternative to natural soils because of the optical and physical properties presented by this material, which benefit the use of displacement tracking methods.

ACKNOWLEDGMENTS

The researchers gratefully acknowledge the funding provided by HUESKER Inc. to conduct this investigation. The authors would also like to thank the anonymous reviewers whose comments and suggestions helped improve and clarify this manuscript.

References

Ads, A., M. Iskander, and S. Bless. 2020. "Shear Strength of a Synthetic Transparent Soft Clay Using a Miniature Ball Penetrometer Test." *Geotechnical Testing Journal* 43, no. 5 (October): 1248–1268. https://doi.org/10.1520/GTJ20190020

ASTM International. 2018. *Standard Specification for Reagent Water*. ASTM D1193-06(2018). West Conshohocken, PA: ASTM International, approved March 15, 2018. https://doi.org/10.1520/D1193-06R18

Balnois, E., S. Durand-Vidal, and P. Livitz. 2003. "Probing the Morphology of Laponite Clay Colloids by Atomic Force Microscopy." *Langmuir* 19, no. 17 (July): 6633–6637. https://doi.org/10.1021/la0340908

Barnes, H. A. 1997. "Thixotropy – A Review." *Journal of Non-Newtonian Fluid Mechanics* 70, nos. 1–2 (May): 1–33. https://doi.org/10.1016/S0377-0257(97)00004-9

Beemer, R. D. and C. P. Aubeny. 2012. "Digital Image Processing of Drag Embedment Anchors in Translucent Silicate Gel." In *GeoManitoba 2012*, 1–8. Richmond, Canada: Canadian Geotechnical Society.

Beemer, R. D., S. M. Shaughnessy, K. R. Ewert, N. Boardman, G. Biscontin, C. P. Aubeny, and S. M. Grajales. 2016. "The Use of Sodium Pyrophosphate to Improve a Translucent Clay Simulate." In *Geo-Chicago 2016*, 83–93. Reston, VA: American Society of Civil Engineers.

Black, J. A. 2015. "Centrifuge Modelling with Transparent Soil and Laser Aided Imaging." *Geotechnical Testing Journal* 38, no. 5 (September): 631–644. https://doi.org/10.1520/GTJ20140231

Black, J. A. and W. A. Take. 2015. "Quantification of Optical Clarity of Transparent Soil Using the Modulation Transfer Function." *Geotechnical Testing Journal* 38, no. 5 (September): 588–602. https://doi.org/10.1520/GTJ20140216

Blair, D. and E. Dufresne. 2008. "The MatLab Particle Tracking Code Repository: MatLab Particle Tracking." Georgetown University, 2021. http://web.archive.org/web/20210723142548/https://physics.georgetown.edu/

Bonn, D., H. Kellay, H. Tanaka, G. Wegdam, and J. Meunier. 1999. "Laponite: What Is the Difference between a Gel and a Glass?" *Langmuir* 15, no. 22 (September): 7534–7536. https://doi.org/10.1021/la990167+

Brown, M. S. and C. B. Arnold. 2010. "Fundamentals of Laser-Material Interaction and Application to Multiscale Surface Modification." In *Laser Precision Microfabrication*, edited by K. Sugioka, M. Meunier, and A. Piqué, 91–120. Berlin, Germany: Springer Berlin, Heidelberg. https://doi.org/10.1007/978-3-642-10523-4

Chen, J. F., X. P. Guo, J. G. Xue, and P. H. Guo. 2019. "Load Behavior of Model Strip Footing on Reinforced Transparent Soils." *Geosynthetics International* 26, no. 3 (June): 251–260. https://doi.org/10.1680/jgein.19.00003

Chini, C. M., J. F. Wallace, C. J. Rutherford, and J. M. Peschel. 2015. "Shearing Failure Visualization via Particle Tracking in Soft Clay Using a Transparent Soil." *Geotechnical Testing Journal* 38, no. 5 (September): 708–722. https://doi.org/10.1520/GTJ20140210

De Guzman, E. M., and M. C. Alfaro. 2016. "Modelling a Highway Embankment on Peat Foundations Using Transparent Soil." *Procedia Engineering* 143, no. 1 (July): 363–370. https://doi.org/10.1016/j.proeng.2016.06.046

De Guzman, E. M. and M. C. Alfaro. 2018. "Laboratory-Scale Model Studies on Corduroy-Reinforced Road Embankments on Peat Foundations Using Transparent Soil." *Transportation Geotechics* 16, no. 1 (September): 1–10. https://doi.org/10.1016/j.trgeo.2018.05.002

El Howayek, A., A. Bobet, C. T. Johnston, M. Santagata, and J. V. Sinfield. 2014. "Microstructure of Sand-Laponite-Water Systems Using Cryo-SEM." In *Geo-Congress 2014*, 693–702. Reston, VA: American Society of Civil Engineers. https://doi.org/10.1061/9780784413272.067

Ezzein, F. M. and R. J. Bathurst, 2011. "A Transparent Sand for Geotechnical Laboratory Modeling." *Geotechnical Testing Journal* 34, no. 6 (November): 590–601. https://doi.org/10.1520/GTJ103808

Ezzein, F. M. and R. J. Bathurst. 2014. "A New Approach to Evaluate Soil-Geosynthetic Interaction Using a Novel Pullout Test Apparatus and Transient Granular Soil." *Geotextiles and Geomembranes* 42, no. 3 (June): 246–255. https://doi.org/10.1016/j.geotexmem.2014.04.003

Ferreira, J. A. Z. and J. G. Zornberg. 2015. "A Transparent Pullout Testing Device for 3D Evaluation of Soil–Geogrid Interaction." *Geotechnical Testing Journal* 38, no. 5 (September): 686–707. https://doi.org/10.1520/GTJ20140198

Gill, D. R. and B. M. Lehane. 2001. "An Optical Technique for Investigating Soil Displacement Patterns." *Geotechnical Testing Journal* 24, no. 3 (September): 324–329. https://doi.org/10.1520/GTJ11351J

Guzman, I. L., M. Iskander, and S. Bless. 2015. "Observations of Projectile Penetration into a Transparent Soil." *Mechanics Research Communications* 70, no. 1 (December): 4–11. https://doi.org/10.1016/j.mechrescom.2015.08.008

Hecht, E. 2017. *Optics*, 5th ed. Edinburgh, UK: Pearson Education Limited.

Iskander, M. 2010. *Modelling with Transparent Soils*. Berlin, Germany: Springer.

Iskander, M. and J. Liu. 2010. "Spatial Deformation Measurement Using Transparent Soil." *Geotechnical Testing Journal* 33, no. 4 (July): 1–8. https://doi.org/10.1520/GTJ102745

Iskander, M. G., J. Liu, and S. Sadek. 2002. "Transparent Amorphous Silica to Model Clay." *Journal of Geotechnical and Geoenvironmental Engineering* 128, no. 3 (March): 262–273. https://doi.org/10.1061/(ASCE)1090-0241(2002)128:3(262)

Iskander, M. G., S. Sadek, and J. Liu. 2002. "Optical Measurement of Deformation Using Transparent Silica Gel to Model Sand." *International Journal of Physical Modelling in Geotechnics* 2, no. 4 (December): 13–26. https://doi.org/10.1680/ijpmg.2002.020402

Kong, G. Q., L. D. Zhou, Z. T. Wang, G. Yang, and H. Li. 2016. "Shear Modulus and Damping Ratios of Transparent Soil Manufactured by Fused Quartz." *Materials Letters* 182 (November): 257–259. https://doi.org/10.1016/j.matlet.2016.07.012

Kumar, N. V. N. R., K. Muralidhar, and Y. M. Joshi. 2008. "On the Refractive Index of Ageing Dispersions of Laponite." *Applied Clay Science* 42, nos. 1–2 (December): 326–330. https://doi.org/10.1016/j.clay.2007.12.010

Liu, J. and M. G. Iskander. 2010. "Modelling Capacity of Transparent Soil." *Canadian Geotechnical Journal* 47, no. 4 (April): 451–460. https://doi.org/10.1139/T09-116

Liu, J., M. G. Iskander, and S. Sadek. 2003. "Consolidation and Permeability of Transparent Amorphous Silica." *Geotechnical Testing Journal* 26, no. 4 (December): 390–401. https://doi.org/10.1520/GTJ11257J

Lorentz, H. A. 2004. *The Theory of Electrons and Its Applications to the Phenomena of Light and Radiant Heat*. New York: Dover.
McConville, F. X. and S. B. Kessler. 2019. "Scale-Up of Mixing Processes: A Primer." In *Chemical Engineering in the Pharmaceutical Industry: Active Pharmaceutical Ingredients*, 2nd ed., edited by D. J. am Ende and M. T. am Ende, 241–259. Hoboken, NJ: John Wiley & Sons. https://doi.org/10.1002/9781119600800
McKelvey, D., V. Sivakumar, A. Bell, and J. Graham. 2004. "Modelling Vibrated Stone Columns in Soft Clay." *Geotechnical Engineering* 157, no. 3 (July): 137–149. https://doi.org/10.1680/geng.2004.157.3.137
Mitchell, J. K. and K. Soga. 2005. *Fundamentals of Soil Behavior*, 3rd ed. Hoboken, NJ: John Wiley & Sons.
Mossa, S., C. de Michele, and F. Sciortino. 2007. "Aging in Laponite Colloidal Suspension: A Brownian Dynamics Simulation Study." *The Journal of Chemical Physics* 126, no. 1 (January): 1–11. https://doi.org/10.1063/1.2408418
Nelsen, C. W. L. "Experimental Evaluation of Geocell Reinforcement Behavior Using Transparent Soil Techniques." Master's thesis, The University of Texas at Austin, 2018. http://dx.doi.org/10.26153/tsw/1321
Ni, Q., C. C. Hird, and I. Guymer. 2010. "Physical Modelling of Pile Penetration in Clay Using Transparent Soil and Particle Image Velocimetry." *Géotechnique* 60, no. 2 (May): 121–132. https://doi.org/10.1680/geot.8.P.052
Nicolai, T. and S. Cocard. 2000. "Light Scattering Study of the Dispersion of Laponite." *Langmuir* 16, no. 21 (September): 8189–8193. https://doi.org/10.1021/la9915623
Peng, X. and J. G. Zornberg. 2017. "Evaluation of Load Transfer in Geogrids for Base Stabilization Using Transparent Soil." *Procedia Engineering* 189: 307–314. https://doi.org/10.1016/j.proeng.2017.05.049
Peng, X. and J. G. Zornberg. 2019. "Evaluation Soil-Geogrid Interaction Using Transparent Soil with Laser Illumination." *Geosynthetics International* 26, no. 2 (April): 206–221. https://doi.org/10.1680/jgein.19.00004
Ramsay, J. D. F. 1986. "Colloidal Properties of Synthetic Hectorite Clay Dispersions." *Journal of Colloid and Interface Science* 109, no. 2 (February): 441–447. https://doi.org/10.1016/0021-9797(86)90321-8
Ramsay, J. D. F., S. W. Swanton, and J. Bunce. 1990. "Swelling and Dispersion of Smectite Clay Colloids: Determination of Structure by Neutron Diffraction and Small-Angle Neutron Scattering." *Journal of the Chemical Society* 86, no. 23 (December): 3919–3926. https://doi.org/10.1039/FT9908603919
Ruzicka, B. and E. Zaccarelli. 2011. "A Fresh Look at the Laponite Phase Diagram." *Soft Matter* 7, no. 4 (January): 1268–1286. https://doi.org/10.1039/C0SM00590H
Ruzicka, B., L. Zulian, and G. Ruocco. 2006. "More on the Phase Diagram of Laponite." *Langmuir* 22, no. 3 (December): 1106–1111. https://doi.org/10.1021/la0524418
Sadek, S., M. G. Iskander, and J. Liu. 2002. "Geotechnical Properties of Transparent Silica." *Canadian Geotechnical Journal* 39, no. 1 (February): 111–124. https://doi.org/10.1139/t01-075
Sadek, S., M. G. Iskander, and J. Liu. 2003. "Accuracy of Digital Image Correlation for Measuring Deformations in Transparent Media." *Journal of Computing in Civil Engineering* 17, no. 2 (April): 88–96. https://doi.org/10.1061/(ASCE)0887-3801(2003)17:2(88)
Schiebener, P. and J. Straub. 1990. "Refractive Index of Water and Steam as Function of Wavelength, Temperature and Density." *Journal of Physical and Chemical Reference Data* 19, no. 3 (May): 677–717. https://doi.org/10.1063/1.555859
Spiegel, M. R. and L. J. Stephens. 2011. *Statistics*, 4th ed. New York: McGraw-Hill.
Tawari, S. L., D. L. Koch, and C. Cohen. 2001. "Electrical Double-Layer Effects on the Brownian Diffusivity and Aggregation Rate of Laponite Clay Particles." *Journal of Colloid and Interface Science* 240, no. 1 (August): 54–66. https://doi.org/10.1006/jcis.2001.7646
Terzaghi, K., R. B. Peck, and G. Mesri. 1996. *Soil Mechanics in Engineering Practice*, 3rd ed. New York: John Wiley & Sons.
Thielicke, W. and E. J. Stamhuis. 2014. "PIVlab – Towards User-Friendly, Affordable and Accurate Digital Particle Image Velocimetry in MATLAB." *Journal of Open Research Software* 2, no. 1 (October): e30. https://doi.org/10.5334/jors.bl
Thompson, D. W. and J. T. Butterworth. 1992. "The Nature of Laponite and Its Aqueous Dispersions." *Journal of Colloid and Interface Science* 151, no. 1 (June): 236–243. https://doi.org/10.1016/0021-9797(92)90254-J
Toiya, M., J. Hettinga, and W. Losert. 2007. "3D Imaging of Particle Motion during Penetrometer Testing." *Granular Matter* 9, no. 5 (August): 323–329. https://doi.org/10.1007/s10035-007-0044-4
van Olphen, H. 1977. *An Introduction to Clay Colloid Chemistry*, 2nd ed. New York: Interscience Publishers, John Wiley & Sons.
Wallace, J. F. and C. Rutherford. 2015. "Geotechnical Properties of LAPONITE-RD." *Geotechnical Testing Journal* 38, no. 5 (September): 574–587. https://doi.org/10.1520/GTJ20140211
Wallace, J. F., C. Rutherford, and J. Zheng. 2015. "Visualizing Failure Surfaces in Soft Clay due to Suction Caisson Loading." In *2018 IFCEE*, 1–9. Reston, VA: American Society of Civil Engineers. https://doi.org/10.1061/9780784481578.018
White, D. J., W. A. Take, and M. D. Bolton. 2003. "Soil Deformation Measurement Using Particle Image Velocimetry (PIV) and Photogrammetry." *Géotechnique* 53, no. 7 (January): 619–631. https://doi.org/10.1680/geot.53.7.619.37383
Xiang, Y., H. Liu, W. Zhang, J. Chu, D. Zhou, and Y. Xiao. 2018. "Application of Transparent Soil Model Test and DEM Simulation in Study of Tunnel Failure Mechanism." *Tunnelling and Underground Space Technology* 74, no. 1 (April): 178–184. https://doi.org/10.1016/j.tust.2018.01.020
Yi, L.-D., H.-B. Lv, T. Ye, and Y.-P. Zhang. 2018. "Quantification of the Transparency of the Transparent Soil in Geotechnical Modelling." *Advances in Civil Engineering* 2018, no. 10 (September): 1–8. https://doi.org/10.1155/2018/2915924
Yuan, B., M. Sun, L. Xiong, Q. Luo, S. P. Pradhan, and H. Li. 2020. "Investigation of 3D Deformation of Transparent Soil around a Laterally Loaded Pile Based on a Hydraulic Gradient Model Test." *Journal of Building Engineering* 28 (March): 101024. https://doi.org/10.1016/j.jobe.2019.101024